

A Communication-Latency-Aware Co-Simulation Platform for Safety and Comfort Evaluation of Cloud-Controlled ICVs

Yongqi Zhao, Xinrui Zhang, Tomislav Mihalj, Martin Schabauer, Luis Putzer, Erik Reichmann-Blaga, Ádám Boronyák, András Rövid, Gábor Soós, Peizhi Zhang, Lu Xiong, Jia Hu *Senior Member, IEEE*, and Arno Eichberger *Member, IEEE*

Abstract—Testing cloud-controlled intelligent connected vehicles (ICVs) requires simulation environments that faithfully emulate both vehicle behavior and realistic communication latencies. This paper proposes a latency-aware co-simulation platform integrating CarMaker and Vissim to evaluate safety and comfort under real-world vehicle-to-cloud (V2C) latency conditions. Two communication latency models, derived from empirical 5G measurements in China and Hungary, are incorporated and statistically modeled using Gamma distributions. A proactive conflict module (PCM) is proposed to dynamically control background vehicles and generate safety-critical scenarios. The platform is validated through experiments involving an exemplary system under test (SUT) across six testing conditions combining two PCM modes (enabled/disabled) and three latency conditions (none, China, Hungary). Safety and comfort are assessed using metrics including collision rate, distance headway, post-encroachment time, and the spectral characteristics of longitudinal acceleration. Results show that the PCM effectively increases driving environment criticality, while V2C latency primarily affects ride comfort. These findings confirm the platform’s effectiveness in systematically evaluating cloud-controlled ICVs under diverse testing conditions.

Index Terms—Intelligent Connected Vehicles, Co-simulation Platform, 5G, Communication Latency Modeling, Software-in-the-Loop, Simulation Testing.

I. INTRODUCTION

Intelligent connected vehicles (ICVs) utilize vehicle-to-everything (V2X) technology to enable cooperative driving, which enhances traffic efficiency and improves the overall driving experience [1]. Among these, cloud-controlled ICVs further smooth traffic flow through integration of real-time

data exchange with cloud platforms [2]. To support the deployment of such technologies, various countries have introduced strategic initiatives, such as the U.S. Department of Transportation’s “Saving Lives with Connectivity” program [3]. Nevertheless, the large-scale deployment of ICVs requires rigorous testing to ensure their safety and reliability.

At present, three main methods are employed to test ICVs, namely on-road, closed-track, and simulation testing [4]. Although on-road testing provides realism, it is inefficient due to the randomness and uncontrollability of real-world scenarios, requiring billions of miles to sufficiently validate ICVs safety and reliability [5]. Closed-track testing, while efficient and realistic, requires considerable investment in specialized facilities; for example, the ZalaZONE facility in Hungary was built at a cost of 159 million dollars [6]. Simulation testing, which combines efficiency, cost-effectiveness, and realism (when close to reality), has become essential in ICVs development, as exemplified by its significant role in advancing Waymo’s technology [7]. However, rapid advancements in V2X communication for ICVs present evolving challenges for simulation testing.

The testing scope for ICVs has evolved from focusing on individual vehicles to encompassing vehicle-network-cloud systems, where control is managed via cloud platforms. Cloud control involves managing motion planning and control in the cloud, utilizing environmental perception and positioning data from roadside infrastructure and ICVs, as well as transmitting control signals through the network [2]. This architecture requires simulation testing that incorporates vehicle dynamics, driving environments, and network communication latency.

In recent decades, the development of simulators for automated driving has primarily focused on single specific aspects such as traffic flow, sensory data, driving policy or vehicle dynamics, often lacking V2X capabilities [8]. For example, Vissim models realistic traffic flows, but lacks vehicle dynamics, while vehicle dynamics simulators like CarMaker offer detailed vehicle dynamics but cannot simulate traffic flows. To address these limitations and incorporate V2X communication, various software combinations have been proposed, such as NS-3 with Vissim [9], [10] or CarMaker [11], and OMNeT++¹ with SUMO [12] or CARLA [13]. However, these solutions focus on cooperative control systems, emphasizing the improvements of V2X on the traffic efficiency. Due to the scarcity of real-world measurement data, communication latency is frequently treated in a simplified manner.

¹<https://omnetpp.org/>

This work has been submitted to the IEEE for possible publication. Copyright may be transferred without notice, after which this version may no longer be accessible. (*Corresponding author: Xinrui Zhang*)

Yongqi Zhao is with the School of Automotive Studies, Tongji University, Shanghai 201804, China and the Institute of Automotive Engineering, Graz University of Technology, Graz 8010, Austria (e-mail: yongqi.zhao@tugraz.at)

Xinrui Zhang, Peizhi Zhang, and Lu Xiong are with the School of Automotive Studies, Tongji University, Shanghai 201804, China (e-mail: zhangxr@tongji.edu.cn; zhangpeizhitom@126.com; xiong_lu@tongji.edu.cn).

Tomislav Mihalj, Martin Schabauer, Luis Putzer, Erik Reichmann-Blaga, and Arno Eichberger are with the Institute of Automotive Engineering, Graz University of Technology, Graz 8010, Austria (e-mail: tomislav.mihalj@tugraz.at; martin.schabauer@tugraz.at; putzer@alumni.tugraz.at; e.reichmannblaga@gmail.com; arno.eichberger@tugraz.at).

Ádám Boronyák and András Rövid are with Department of Automotive Technologies, Budapest University of Technology and Economics, Budapest, 1111, Hungary (e-mail: boronyak.adam@kjk.bme.hu; rovid.andras@kjk.bme.hu).

Gábor Soós is with Magyar Telekom Nyrt., Budapest, 1097, Hungary (e-mail: soos.gabor2@telekom.hu).

Jia Hu is with Key Laboratory of Road and Traffic Engineering of the Ministry of Education, Tongji University, Shanghai 201804, China (e-mail: hujia@tongji.edu.cn).

In addition to software, hardware components have also been integrated into simulation platforms to enhance fidelity. Real test vehicles [14], [15] and driving simulators [16] simulate the vehicle dynamics, while augmented reality, traffic simulator, and real traffic are used to model background vehicles [14]–[17]. Cohda wireless device and V2X signal generator have been utilized to establish V2X communication [14], [16], [18], [19].

In summary, three limitations are evident in existing simulation platforms. First, vehicle dynamics and traffic flow are often handled separately, with few platforms integrating both and frequently lacking V2X simulation, which makes ICVs testing infeasible. Second, the absence of real-world communication latency data has constrained research on its effects. Third, testing efficiency is limited, as the ego vehicle is generally exposed to a low critical driving environment, reducing interaction with challenging scenarios.

To address the identified limitations, a co-simulation platform has been developed with the following contributions:

- 1) Simulations of vehicle dynamics, traffic flow, and vehicle-to-cloud (V2C) communication are achieved by integrating CarMaker and Vissim.
- 2) The vehicle dynamics model and traffic flow are built upon real measurements, while two V2C communication latency models, based on data collected in China and Hungary, are implemented to represent realistic communication latencies for different use cases.
- 3) The V2C communication latency distributions are statistically fitted to measurement data and further validated through analytical derivation to follow Gamma distributions.
- 4) Background vehicles (BGVs) are strategically controlled to ensure higher exposure to critical driving scenarios, thereby enhancing testing efficiency.
- 5) The effects of varying V2C communication latencies on ICVs are systematically investigated and analyzed.

A tool is described for simulating critical driving scenarios with realistic communication latencies, aiding the development of robust ICVs algorithms. Safety and comfort performance under diverse latency conditions is also facilitated.

II. RELATED WORK

Since the 1990s, simulation platforms tailored for the development and validation of automated driving systems (ADSs) have gained increasing importance. They offer significant advantages by reducing the need for extensive on-road testing and accelerating the verification and validation process. Over the past three decades, numerous simulators have been developed for various purposes, including traffic control design, sensor data processing, driving policy formulation, vehicle dynamics optimization, and vehicle control. However, these simulators are typically specialized, often focusing on a single aspect, such as vehicle dynamics or traffic flow, without providing integrated solutions. Furthermore, contributions to the simulation of V2X communication have been relatively limited. [8]

In response to these limitations, co-simulation frameworks have been proposed, which integrate multiple tools for

more comprehensive simulations. Most frameworks combine a mainstream simulator (e.g., Vissim, SUMO, CARLA, or CarMaker) with a third-party software to address specific gaps. For example, Vissim, proficient in simulating traffic flow but lacking V2X functionality, was integrated with MATLAB for platoon control and NS-3 for communication constraints [9], [10]. Similarly, SUMO was combined with TraaS [20], and OMNeT++ [12] to enable V2X simulation. CARLA was extended through Python API expansion [21], [22], OMNeT++ [13], and Artery V2X [23] for V2X functionality. Other notable efforts include OpenCDA, which integrates CARLA with SUMO [24], and a framework combining NS-3 and CarMaker for V2X simulation [11]. Nalic et al. [25] developed a co-simulation framework to generate critical scenarios, yet not supporting V2X functionality. Additionally, Gazebo was employed to build V2X-compatible simulation platforms [26], and [27] recently introduced a simulation platform for truck platoon management.

In addition to software-only simulations, vehicle-in-the-loop (ViL) approach was integrated to enhance simulation realism. Eichberger et al. [14] employed a vehicle equipped with a Cohda MK4 device to gather V2X communication data and develop a sensor model, while Peters et al. [17] used a Cohda MK6² device to establish a C-V2X platform. Lei et al. [18] designed an in-chamber test scheme using a real vehicle and an CMW 500³ signal generator for V2X evaluations. Feng et al. [15] combined a real vehicle with augmented reality in a ViL setup, although without V2X functionality.

Hardware-in-the-loop (HiL) approaches integrate real hardware into simulation frameworks, offering realistic environments for system testing and validation. Lee et al. [16] developed a HiL simulator based on dSPACE and Cohda MK5 to evaluate cooperative eco-driving systems. Mafakheri et al. [28] implemented real-time HiL simulations with SUMO and a roadside unit to examine interactions between test vehicles and simulated objects. Wang et al. [19] introduced a laboratory framework combining VTD and RF generator for V2X evaluations, while Gemmi et al. [29] used SUMO with Colosseum network emulator (cf. [30]) to simulate cooperative, connected, and automated mobility scenarios.

In summary, the reviewed simulation platforms are unable to fully support ICV testing due to their limitations in integrating vehicle dynamics, traffic flow, realistic V2C communication models with latency considerations and efficient exposure to critical driving scenarios. To overcome these drawbacks, a simulation platform combining CarMaker, Vissim and V2C communication latency measurements is proposed in the present work.

III. METHODOLOGY

Figure 1 illustrates the architecture of the proposed co-simulation platform. It integrates the system under test (SUT) hosted in a cloud emulator in Simulink environment (cf. Section III-A), with a traffic environment modeled in Vissim,

²<https://www.cohdawireless.com/solutions/mk6/>

³https://www.rohde-schwarz.com/nl/products/test-and-measurement/wireless-tester-network-emulator/rs-cmw500-wideband-radio-communication-tester_63493-10844.html

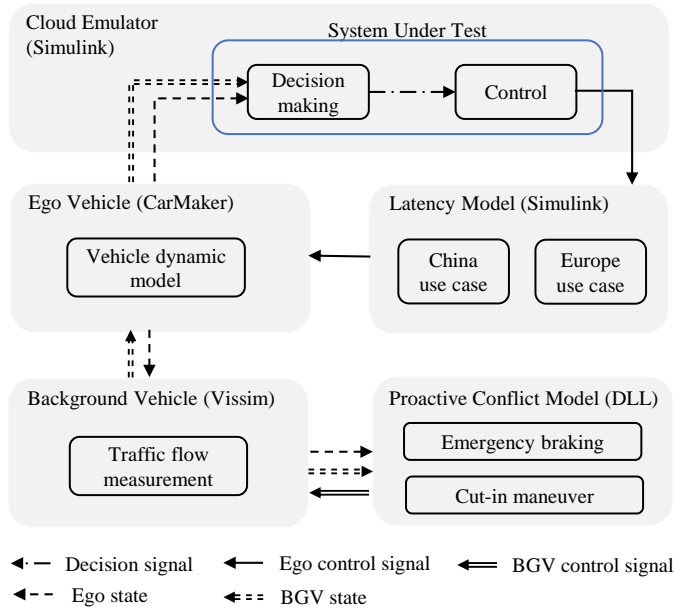


Figure 1. The architecture of the proposed co-simulation platform.

where BGVs can be controlled dynamically (cf. Section III-C). A proactive conflict model (PCM), implemented via a driver model dynamic link library (DLL), enables the manipulation of BGVs in Vissim to generate critical testing scenarios (cf. Section III-D). The ego vehicle is simulated in CarMaker using a detailed vehicle dynamics model (cf. Section III-B). In addition, a V2C communication latency model formulated by integrating empirical fitting from real-world 5G measurements and analytical derivation is included to emulate realistic communication delays (cf. Section III-E).

A. Cloud Emulator

The cloud environment is emulated within Simulink, serving as the deployment platform for the SUT, as illustrated in Figure 1. The SUT represents a Level 2 ADS, classified according to the SAE taxonomy [31]. BGVs detection is performed through an ideal sensor installed on the ego vehicle. The term “ideal sensor” denotes the acquisition of ground truth data, such as positions and velocities, rather than raw sensor outputs. The states of the detected BGVs and the ego vehicle are transmitted to the cloud in real time. Subsequently, control signals are relayed from the cloud to the ego vehicle, incorporating the effects of communication latency.

B. Ego Vehicle

A three-dimensional nonlinear vehicle model of a BMW 640i Gran Coupe (2011), which serves as test vehicle, was built in IPG CarMaker. At first, necessary model parameters and characteristics, see Table I, were identified by laboratory measurements as well as data sheets and reasonable approximations, in cases where no measurement or data was available. Subsequently, active subsystems, such as active steering, which were not available as template in CarMaker,

were modeled separately in MATLAB/Simulink and implemented. Finally, the vehicle model and simulation results were evaluated and experimentally validated by means of measurement data obtained by real-world vehicle dynamics testing conducted on a proving ground. In Appendix A, the main topics of building and evaluating the vehicle model are summarized and the validation results are briefly described.

Table I
REQUIRED PARAMETERS AND CHARACTERISTICS OF THE VEHICLE MODEL.

Module	Parameters & characteristics
General	Mass
	Moments of inertia
	Center of gravity
Steering system	Steering ratio
Suspension system	Spring characteristics
	Damping characteristics
	Anti-roll bar characteristics
	Suspension kinematics
Tires	Tire force characteristics
Power train	Engine characteristics
	Transmission ratio
	Drive system inertia
	Brake system characteristics

C. Background Vehicle

To accurately represent real traffic density in the proposed simulation platform, comprehensive cross-sectional measurements were conducted across the road network under test depicted in Figure 2. Laser scanners and additional measurement devices were placed at various points along the highway, capturing data on vehicle counts, speed distributions, and vehicle classifications. This dataset is essential for formulating the traffic model to reflect naturalistic traffic flow conditions. Further details on the collected data can be found in our previous work [25].

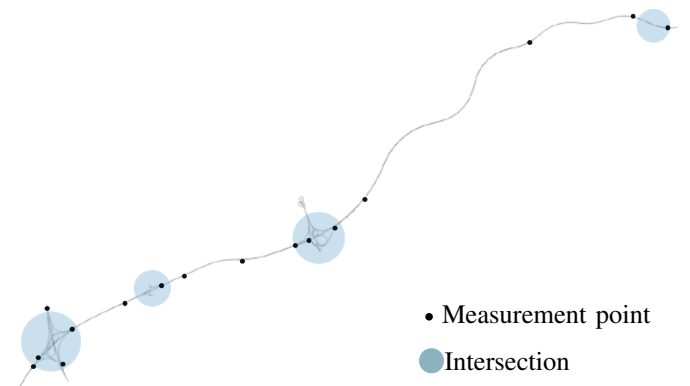


Figure 2. Overview of the road network under test [25].

D. Proactive Conflict Module

The PCM utilizes the Vissim’s driver model application programming interface (API) to create challenging scenarios

by customizing BGV behaviors. Through integrating a driver model DLL in C code, default driving logic is overridden, enabling real-time control of acceleration, braking, and lane changes. Two conflict-inducing behaviors are implemented: an unintended emergency brake by the lead vehicle and a cut-in by an adjacent vehicle.

1) *Emergency Braking*: A BGV traveling ahead of the ego vehicle in the same lane is designated as the lead vehicle. The distance d between the two vehicles is computed by

$$d(t) = \|\mathbf{p}_{\text{lead}}(t) - \mathbf{p}_{\text{ego}}(t)\|, \quad (1)$$

where $\mathbf{p}_{\text{lead}}(t)$ and $\mathbf{p}_{\text{ego}}(t)$ denote the positions of the lead and ego vehicles at time t , respectively, and $\|\cdot\|$ denotes the standard Euclidean norm. When its distance to the ego falls below a defined threshold D_{brake} , i.e., $d(t) < D_{\text{brake}}$, the lead vehicle applies a sudden deceleration to simulate an emergency brake, thereby assessing the SUT's ability to respond under critical following scenarios.

2) *Cut-in Maneuver*: BGVs in adjacent lanes are evaluated based on their Euclidean distance to the ego vehicle d_i , which is given by

$$d_i(t) = \|\mathbf{p}_i(t) - \mathbf{p}_{\text{ego}}(t)\|, \quad (2)$$

where $\mathbf{p}_i(t)$ denotes the position of the i -th BGV. A BGV is considered a potential cut-in candidate if its distance to the ego vehicle falls below a predefined threshold D_{cut} , i.e.,

$$\mathcal{C} = \{i \mid d_i(t) < D_{\text{cut}}\} \quad (3)$$

where \mathcal{C} represents the set of all such candidate BGVs, and D_{cut} is the predefined spatial threshold. Among all candidates, the closest BGV is selected by

$$i^* = \arg \min_{i \in \mathcal{C}} d_i(t). \quad (4)$$

The selected BGV i^* then performs a lane-change maneuver into the ego vehicle's lane, introducing a lateral encroachment. This scenario challenges the SUT's perception and decision-making modules in dynamically evolving environments.

E. Latency Model

Communication latency is often simulated using analytical models, though their reliance on external tools and limited fidelity hinder co-simulation [32], [33]. To address this, two probabilistic models are developed using real-world measurements from China and Europe [34], [35].

1) *Overview of 5G Network Architecture*: Figure 3 illustrates the 5G network architecture used in the China and Europe cases. In both, the core components include the on-board unit (OBU), next-generation Node B (gNB), user plane function (UPF), and application server (AS), enabling V2C communication. The European architecture further incorporates a vehicle-to-infrastructure (V2I) link via roadside units (RSUs), supporting cooperative perception between vehicle and infrastructure.

The latency components in Figure 3 are denoted as l_{V2I} , l_{radio} , l_{TN} , l_{CN} , $l_{\text{UPF-AS}}$, and l_{AS} , representing the delays introduced by V2I communication, wireless transmission, transport network, core network, UPF to AS communication,

and AS processing, respectively. The V2I link (l_{V2I}) is unique to the Europe use case and enables direct interaction between the ego vehicle and RSUs. Additionally, arrows in the figure represent bidirectional data communication.

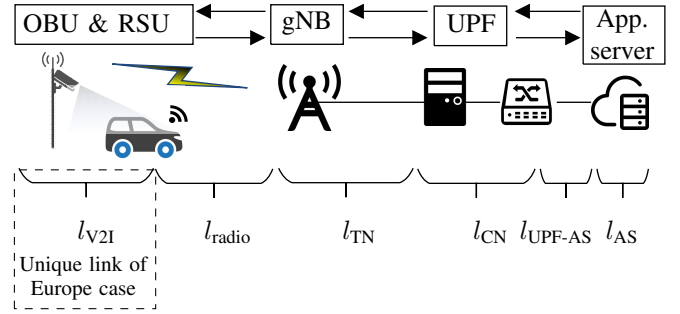


Figure 3. Common network architecture in China and Europe.

2) China Use Case:

Overview of V2X Solution: The process of vehicle-cloud interaction is illustrated in Figure 4. Real-time vehicle state data are transmitted to a 5G base station (gNB) and routed through the core network to a cloud control center, where optimized trajectories are computed and sent back to the vehicle via the same 5G infrastructure.

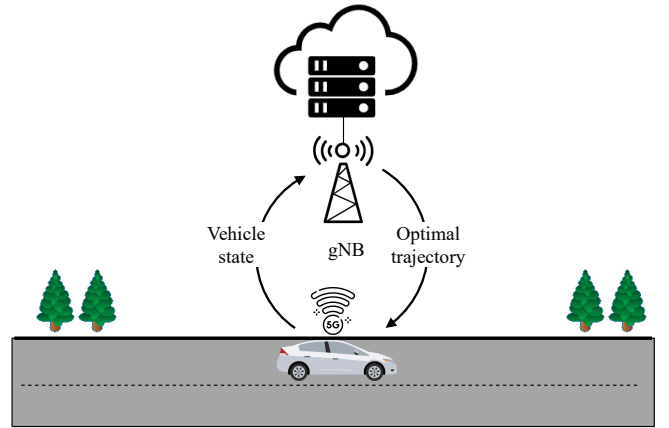


Figure 4. V2X communication solution in China use case.

Probabilistic Model: A measurement campaign was conducted at the ICV testing base of Tongji University, in Shanghai, China. Tests were performed at stand still 0 km/h, as well as 20 km/h and 40 km/h traveling velocity. To enhance data reliability, each scenario was repeated at least ten times. Figure 5a–5c present the empirical latency distributions alongside fitted curves based on Gamma, Normal, Nakagami, and Rayleigh models. The quality of fit is evaluated using the sum of squared errors (SSE). As indicated in Table II, the **Gamma distribution** consistently achieved the lowest SSE across all test cases, demonstrating superior fitting performance.

3) Europe Use Case:

Overview of V2X Solution: As shown in Figure 6, the European V2X architecture comprises three main components: the RSU, test vehicle, and the central server (CS) that functions as a cloud-based processing unit. The RSU integrates sensors

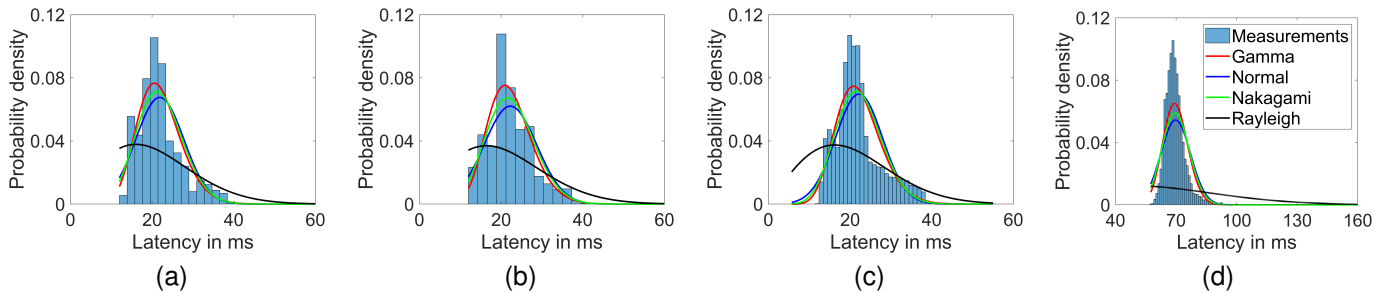


Figure 5. Measured latency and fitted distributions of China cases with 0 km/h (5a), 20 km/h (5b), 40 km/h (5c) and Europe cases (5d).

Table II
SSE BETWEEN MEASURED AND FITTED LATENCY DISTRIBUTIONS

Velocity (km/h)	SSE			
	Normal	Nakagami	Rayleigh	Gamma
0	0.0265	0.0226	0.0688	0.0185
20	0.0053	0.0047	0.0058	0.0038
40	0.0091	0.0075	0.0080	0.0066

***Bold entries** indicate the distribution with the lowest SSE, indicating the best fit to the measurements.

and an edge computer for object detection and tracking, forwarding the results to the CS. The test vehicle communicates its position to the CS and receives control signals for trajectory adjustment. A fusion algorithm within the CS combines inputs from both sources, which are then used by the trajectory planner to compute and return optimized trajectories. Further architectural details are provided in [36]–[38].

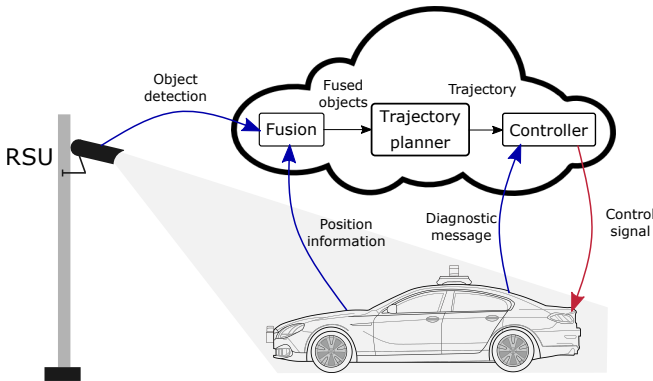


Figure 6. V2X communication solution in Europa use case.

Probabilistic Model: The measurement campaign was conducted at the ZalaZONE⁴ proving ground in Zalaegerszeg, Hungary [39]. The scenario involved a cloud-based control system reacting to a pedestrian dummy crossing as the test vehicle approached. The RSU monitored the scenario and relayed the data to the CS, simulating the cloud functionality. The CS then transmitted control signals to the vehicle to initiate an evasive maneuver.

The latency distribution for the European use case is based on five test trials, each lasting approximately 120 s and involv-

⁴<https://zalazone.hu/en/>

ing the exchange of about 1200 messages exchanged between the test vehicle and the CS. Figure 5d shows the measured latency distribution along with fitted models, and Table III summarizes the SSE-based evaluation. Consistent with the China case results, the **Gamma distribution** again yields the best fit.

Table III
SSE BETWEEN MEASUREMENTS AND FITTED DISTRIBUTIONS

Model	Normal	Nakagami	Rayleigh	Gamma
SSE	0.0080	0.0063	0.0258	0.0044

***Bold entry** indicates the distribution with the lowest SSE, indicating the best fit to the measurements.

4) *Theoretical Model:* To further validate the probabilistic model, a theoretical latency model is developed based on the structure of 5G communication networks. It incorporates queuing theory and retransmission mechanisms to analytically characterize latency. The derived latency distribution aligns with the **Gamma distribution**, thereby substantiating the empirical findings. The complete derivation process is detailed in Appendix B.

IV. EXPERIMENT

In Section III, the methodology to construct the co-simulation platform is introduced, and a snippet of its implementation is shown in Figure 7. In this section a simulation experiment is conducted and the results are analyzed to demonstrate the validity of this platform.

A. Simulation Setup

Table IV presents the simulation test matrix, comprising six conditions, defined by two PCM configurations (with and without PCM) and three latency profiles: no latency (NL), China latency (CL), Hungary latency (HL).

Each condition was evaluated under multiple initial configurations of the ego vehicle. These include five speeds and three lane positions, as summarized in Table IV. A simulation run refers to a complete run over the predefined scenario duration, which continues regardless of any collision occurrence.

B. Safety Assessment

The safety performance of the SUT is assessed using three complementary metrics: the collision rate (CR), the distance

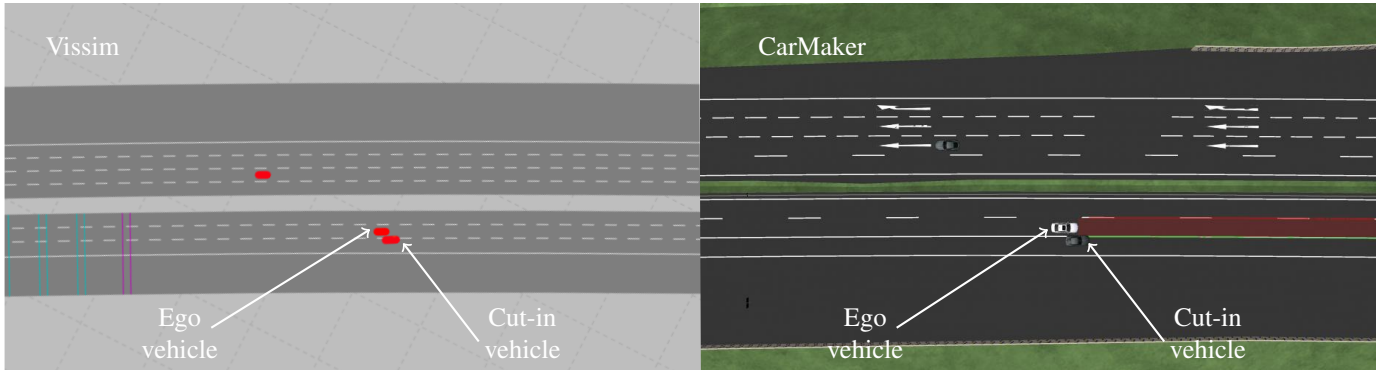


Figure 7. A snippet of a cut-in scenario in the co-simulation platform, where the cut-in vehicle is controlled by the PCM. The Left image shows the simulation in Vissim, while the right image presents the simulation in CarMaker.

Table IV
SIMULATION TEST MATRIX

	NL	CL	HL
Without PCM	✓	✓	✓
With PCM	✓	✓	✓

*Each condition was simulated across five initial speeds (90, 100, 110, 120, 130 km/h) and three initial lane positions (left, center, right).

headway (DHW), and the post-encroachment time (PET). The CR measures the frequency of collisions to reflect overall safety. The DHW assesses the criticality of following scenarios, while the PET characterizes the criticality of cut-in scenarios encountered by the ego vehicle.

1) Collision Rate:

Metric Definition: The CR is computed cumulatively across all simulation runs by

$$CR = \frac{\sum_{i=1}^n N_{\text{collision}}^{(i)}}{\sum_{i=1}^n D^{(i)}}, \quad (5)$$

where $N_{\text{collision}}^{(i)}$ denotes the number of collisions in the i -th simulation run, $D^{(i)}$ is the driving distance in kilometers for the i -th run, and n represents the total number of runs.

Assessment Result: Figure 8 illustrates the CR under six test conditions. A markedly higher CR is observed when PCM is activated compared to tests without PCM across all latency settings. This suggests that the PCM effectively generates high-risk scenarios, thereby accelerating the exposure of the SUT to safety-critical scenarios.

When PCM is disabled, CR remains low and shows no variation across latency profiles. When PCM is active, CR under NL, CL, and HL are comparable. These findings indicate that latency cannot directly lead to collisions of ICVs in non-extreme scenarios, which aligns with previous work [40].

2) Distance Headway:

Metric Definition: In following scenarios, the DHW denotes the Euclidean distance between the ego and the lead vehicle at each time step, defined as

$$DHW(t) = \|\mathbf{p}_{\text{lead}}(t) - \mathbf{p}_{\text{ego}}(t)\|, \quad (6)$$

where $\mathbf{p}_{\text{lead}}(t)$ and $\mathbf{p}_{\text{ego}}(t)$ denote the positions of the lead and ego vehicles at time t , respectively. Based on [41], a

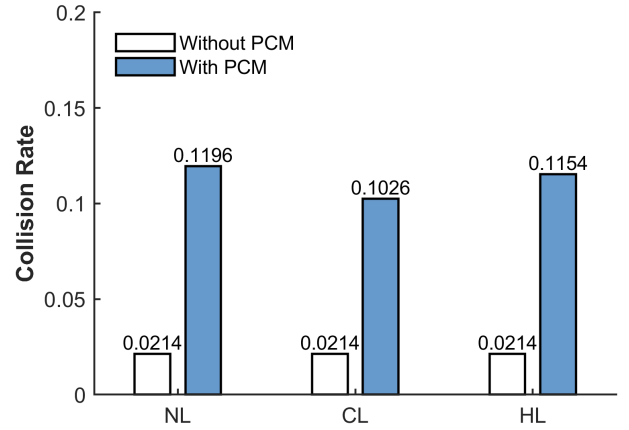


Figure 8. Collision rate of simulation test.

highway following scenario is considered critical when the DHW falls below 50 m. Then, the frequency of a critical following scenario $f_{\text{crit}}^{\text{DHW}}$ is computed by

$$f_{\text{crit}}^{\text{DHW}} = \frac{N_{\text{DHW} < 50}}{N_{\text{total}}}, \quad (7)$$

where $N_{\text{DHW} < 50}$ is the number of time steps with DHW below 50 m, and N_{total} is the total number of time steps during the simulation.

Assessment Result: Table V presents the frequency of critical following scenarios $f_{\text{crit}}^{\text{DHW}}$ under each test condition. With PCM activated, the frequency increases by 1.2 to 1.5 times compared to when PCM is disabled, indicating that PCM substantially elevates the criticality of following scenarios.

Table V
FREQUENCY OF CRITICAL FOLLOWING SCENARIOS

	NL	CL	HL
Without PCM	0.199	0.205	0.199
With PCM	0.484	0.465	0.508
Increase	+143.2%	+126.8%	+155.3%

***Bold values** indicate the percentage increase in the frequency of critical following scenarios caused by PCM activation.

Table VI reports the relative changes in frequency of critical following scenarios compared to the NL condition. No

consistent pattern is observed regarding the effect of latency, regardless of whether PCM is enabled or not, suggesting that latency has limited impact on causing critical following scenarios.

Table VI
RELATIVE CHANGE IN CRITICAL FOLLOWING SCENARIO FREQUENCY (NL VS. OTHERS)

Comparison	Without PCM	With PCM
NL vs. CL	+3.0%	-3.9%
NL vs. HL	0.0%	+5.0%

***Bold values** indicate the percentage increase in critical following scenario frequency, computed by comparing CL, and HL against the NL baseline.

3) Post-Encroachment Time:

Metric Definition: In cut-in scenarios, the PET quantifies the temporal gap between the completion of a cut-in vehicle's lane change and the ego vehicle reaching the same location, with a defined spatial tolerance δ . PET is computed by

$$PET = t_{ego} - t_{cut}, \quad (8)$$

where t_{cut} is the time when the cut-in vehicle completes the maneuver and t_{ego} is the earliest time when the ego vehicle reaches the same location (within δ). Let \mathbf{p}_{cut}^* be the position of the cut-in vehicle at time t_{cut} , then

$$t_{ego} = \min \{t \geq t_{cut} \mid \|\mathbf{p}_{ego}(t) - \mathbf{p}_{cut}^*\| < \delta\}. \quad (9)$$

Following [42], a cut-in scenario is regarded as critical if the PET is below 1 s. Then, the frequency of critical cut-in scenarios f_{crit}^{PET} is computed by

$$f_{crit}^{PET} = \frac{N_{PET < 1s}}{N_{cut-in}}, \quad (10)$$

where $N_{PET < 1s}$ is the number of cut-in scenarios with PET below 1 s, and N_{cut-in} is the total number of cut-in scenarios during the simulation.

Assessment Result: Table VII summarizes the frequency of critical cut-in scenarios f_{crit}^{PET} under different test conditions. A marked increase is observed when PCM is activated, indicating that the PCM effectively generates high-risk cut-in scenarios on highways.

Table VII
FREQUENCY OF CRITICAL CUT-IN SCENARIOS

	NL	CL	HL
Without PCM	0.132	0.143	0.132
With PCM	0.343	0.312	0.320
Increase	+159.8%	+118.2%	+142.4%

***Bold values** indicate the percentage increase in the frequency of critical cut-in scenarios caused by PCM activation.

Table VIII reports the relative changes in critical cut-in scenario frequency. The results suggest that CL and HL exhibit inconsistent effects on enhancing criticality of cut-in scenarios, regardless of PCM activation. This indicates that the effect of latency on ICV safety performance cannot be substantiated through enhancing criticality in cut-in scenarios.

Table VIII
RELATIVE CHANGE IN CRITICAL CUT-IN SCENARIO FREQUENCY (NL VS. OTHERS)

Comparison	Without PCM	With PCM
NL vs. CL	+8.3%	-9.0%
NL vs. HL	0.0%	-6.7%

***Bold values** indicate the percentage increase in critical cut-in scenario frequency, computed by comparing CL and HL against the NL baseline.

C. Comfort Assessment

1) *Metric Definition:* The comfort metric is defined as the total energy of longitudinal acceleration within the ISO 2631-defined sensitive frequency band (0.5–10 Hz) [43], obtained via discrete Fourier transform (DFT) of the absolute acceleration signal. The power spectral density $P(f)$ is calculated by

$$P(f) = \frac{|\mathcal{F}(a(t))|^2}{N}, \quad (11)$$

where $a(t)$ is the absolute longitudinal acceleration, $\mathcal{F}(a(t))$ is its Fourier transform, N is the number of samples. The total power in sensitive frequency band E_{sens} is then computed by summing $P(f)$ over the range of $f \in [0.5, 10]$ Hz

$$E_{sens} = \sum_{f=0.5 \text{ Hz}}^{10 \text{ Hz}} P(f). \quad (12)$$

2) *Assessment Result:* Table IX presents the total power within sensitive frequency across all test conditions. The results show that PCM activation leads to a substantial increase in power compared to the no-PCM case. This indicates that PCM significantly degrades ride comfort.

Table IX
TOTAL POWER WITHIN SENSITIVE FREQUENCY ((m/s²)²)

	NL	CL	HL
Without PCM	6566.51	6796.71	7827.16
With PCM	20522.47	21412.07	24380.87
Increase	+212.6%	+214.9%	+211.4%

***Bold values** indicate the percentage increase in total power in sensitive frequency caused by PCM activation.

Table X presents the relative change in total power within sensitive frequency. The results show that latency increases this power to varying extents under both PCM-on and PCM-off conditions. These findings suggest that latency tends to reduce ride comfort by amplifying longitudinal acceleration in the sensitive frequency range.

Table X
RELATIVE CHANGE IN TOTAL POWER IN SENSITIVE FREQUENCY (NL VS. OTHERS)

Comparison	Without PCM	With PCM
NL vs. CL	+3.5%	+4.3%
NL vs. HL	+19.2%	+18.8%

***Bold values** indicate the percentage increase in total power within sensitive frequency, computed by comparing CL and HL against the NL baseline.

In summary, the following conclusions and findings are obtained through the experiment:

- 1) The proposed co-simulation platform, through the use of the PCM, effectively increases the exposure of the SUT to safety-critical scenarios, particularly by generating more frequent collisions (up to fivefold) and enhancing the criticality of following and cut-in scenarios by 1.2 to 1.5 times. This demonstrates the platform's capability in accelerating safety validation.
- 2) V2C communication latency does not significantly affect the safety performance of ICVs. It neither increases the collision rate nor intensifies the criticality of following or cut-in scenarios. However, it consistently reduces ride comfort by amplifying longitudinal acceleration within the sensitive frequency range, leading to power increases of up to 20%. This finding is consistent with the observation reported in [40].

V. CONCLUSION

This study introduces a co-simulation platform that combines a detailed vehicle dynamics model, a realistic traffic environment based on real-world measurements, strategic BGV control, and a V2C latency model for assessing ICVs. The platform's validity is demonstrated through testing an exemplary SUT across six conditions, combining PCM activation with three latency settings. The simulation results indicate that the platform can generate high-risk driving environments, resulting in approximately a fivefold increase in collisions and 1.2 to 1.5 times more safety-critical following and cut-in scenarios. Moreover, the results reveal that V2C communication latency has a primary impact on ICV comfort rather than safety performance, which is consistent with findings reported in [40].

A practical limitation of the platform is slower simulation speed when the PCM is activated to control BGVs, as frequent data exchange introduces delays. Improving the communication interface or running the controller in parallel can speed up the simulation.

In future research, critical scenarios formatted with Open-SCENARIO, generated using the tool developed in [44], will be incorporated to enable scenario-based testing. Additionally, Vehicle-to-Infrastructure (V2I) cooperative perception will be incorporated to address perception limitations and information silos.

APPENDIX A VEHICLE DYNAMICS MODEL

A. Parameter identification

The required model parameters and characteristics are outlined in Table I. In the following, the main topics of the identification process are summarized.

- **Mass and center of gravity (COG):** Parameters were experimentally identified by laboratory measurements, applying the method of [45]. The total mass as well as the position of the COG in longitudinal and lateral direction were determined by wheel load measurements on scales

on a flat surface. The height of the COG (vertical direction) was determined by lifting one axle of the vehicle.

- **Moments of inertia (MOI):** Measurement of the inertia tensor of the specific test vehicle was not possible. However, data of measured MOI of a reference vehicle was available. Therefore, the MOI regarding the pitch, roll and yaw motions were approximated in a simple but effective approach. The respective measured values of the reference vehicle I_{ref}^{meas} were compared to the value of an idealized rigid cuboid I_{ref}^{cub} , approximating the overall size of the reference vehicle, by

$$i_{corr} = \frac{I_{ref}^{meas}}{I_{ref}^{cub}}. \quad (13)$$

Additionally, it was assumed that the ratio described by the dimensionless correction factor i_{corr} is similar for the test vehicle. Hence, the MOI of the test vehicle I_{ego}^{approx} were approximated by

$$I_{ego}^{approx} = I_{ego}^{cub} i_{corr}, \quad (14)$$

where I_{ego}^{cub} represents the MOI of a cuboid with the size of the test vehicle.

- **Spring characteristics:** Suspension spring characteristics and stiffness were experimentally identified by laboratory measurements, applying the method of [46]. The test vehicle was loaded with additional weights in certain stages, which lead to increasing wheel loads and vertical suspension travel. The wheel loads were measured by scales and the vertical suspension travel by cable-extension transducers positioned at each wheel. Consequently, spring characteristics were determined and the stiffness identified. This pragmatic and effective approach leads to sufficiently accurate results, avoiding cumbersome and expensive measurements on test rigs.
- **Damping characteristics:** Measurement of suspension damping characteristics was not possible. Additionally, the test vehicle is equipped with an active damping system, where no data was available. Therefore, suspension damping properties c_s were approximated based on the dimensionless damping ratio ζ , assuming simple vertical dynamics of a quarter vehicle (one mass oscillator) by

$$\zeta = \frac{c_s}{2\sqrt{k_s m}}, \quad (15)$$

where m denotes a quarter of the total vehicle mass and k_s indicates the suspension spring stiffness. A sportive design was assumed and different damping properties for compression and rebound cycles, resulting in overall nonlinear damping characteristics.

- **Anti-roll bar characteristics:** The test vehicle is equipped with actively controlled anti-roll bar characteristics on the front as well as on the rear axle. No information about the active system was available. Therefore, anti-roll bar characteristics were modeled by pragmatic approaches, resulting in a vehicle velocity and lateral acceleration dependent anti-roll bar stiffness. These, characteristics were identified using measurement data of closed-track vehicle dynamics testing on a proving ground.

- **Steering ratio:** The test vehicle is equipped with active front and rear wheel steering. In a first step, steering characteristics and the steering ratio were experimentally identified by laboratory measurements in standstill. Measurements were carried out with a measurement steering wheel and wheel protractors. Subsequently, the identified steering ratio in standstill was adjusted for the active, velocity dependent steering system, based on closed-track vehicle dynamics testing on a proving ground.
- **Tire force characteristics:** Data of the test vehicle's tires was not available. Therefore, measured tire force characteristics of a similar tire, obtained by tire testing on an industrial flat track tire test rig, were used. Similar tire properties were assumed.
- **Powertrain characteristics:** Power and torque characteristics, as well as gear ratios, were obtained from the data sheet of the vehicle.

B. Modeling of subsystems and implementation

The adaptable multi-body framework of CarMaker was used to consider the actively controlled subsystems of the test vehicle, in particular the active anti-roll bars as well as the front and rear wheel steering systems. These systems were modeled in MATLAB/Simulink, based on measurement data from closed-track vehicle dynamics measurements and implemented as Functional Mock-up Units (FMUs) in CarMaker. Tire force transmission was modeled by Pacejka's Magic Formula tire model, which is directly available in CarMaker. For the remaining subsystems and characteristics, such as brake system and suspension kinematics, generic templates of CarMaker were used.

C. Evaluation and experimental validation

The performance of the vehicle model as well as the plausibility of simulation results were evaluated and validated by means of vehicle dynamics measurement data. Tests were conducted on a closed-track proving ground, including steady-state cornering on a 90 m circular track, sinusoidal steering maneuvers at 55 km/h and 80 km/h as well as different acceleration and braking maneuvers, see [47].

Measurement data was collected using a Genesys ADMA⁵ device, which recorded speeds, accelerations, position, and attitude angles. Additionally, the steering wheel angle was measured by a measurement steering wheel.

Subsequently, measurements and simulation results were compared by using measured steering angle and vehicle speed as inputs for the model, to replicate the closed-track tests. In Table XI, the calculated Root Mean Square Errors (RMSEs) between measurement and simulation results of relevant quantities are listed, such as longitudinal velocity v_x , yaw rate ω_z , roll angle ϕ as well as longitudinal and lateral accelerations a_x and a_y , respectively.

Although there are higher deviations of the yaw rate, especially during sinusoidal steering, and further validations are recommended, the overall results indicate that the vehicle

model is valid for the investigations conducted in the present work.

Table XI
RMSE BETWEEN SIMULATION RESULTS AND MEASUREMENTS, BASED ON [47].

RMSE	Steady-state cornering	Sinusoidal steering	Acceleration maneuver
v_x (km/h)	0.48	0.38	0.58
a_x (m/s ²)	0.31	0.68	0.55
a_y (m/s ²)	0.23	0.56	0.31
ω_z (°/s)	0.93	3.49	1.01
ϕ (°)	0.30	0.34	NA

APPENDIX B THEORETICAL LATENCY MODEL

The theoretical latency model is derived and validated against the actual communication latency depicted in Figure 3. The end-to-end (E2E) 5G communication latency l_{E2E} includes the radio access network (RAN) l_{radio} , transport network (TN) l_{TN} , core network (CN) latency l_{CN} , the latency between the CN' UPF node and the AS l_{UPF-AS} , and the AS processing latency l_{AS} . This is expressed as

$$l_{E2E} = l_{radio} + l_{TN} + l_{CN} + l_{UPF-AS} + l_{AS}. \quad (16)$$

Each of these components includes both uplink and downlink latencies.

In practice, besides considering retransmissions in the RAN, the latencies of other nodes can be simplified to the sum of queuing latency and transmission latency [48]. Therefore, queuing theory is utilized for detailed RAN modeling, while the latencies at other nodes are similar. RAN latency can be formulated as

$$l_{radio} = \tau_{radio} + \tau_{HARQ} + N(\tau'_{radio} + \tau_{HARQ}), \quad (17)$$

with $N = 0, 1, \dots, N_{max}$, and where τ_{radio} and τ'_{radio} are the transmission and retransmission latency between the onboard device and the gNB, respectively. The latency caused by the hybrid automatic repeat request (HARQ) retransmission mechanism is represented by τ_{HARQ} , and N denotes the number of retransmissions. According to the internet protocol (IP) layer data scheduling mechanism, Equation 17 can be reformulated as

$$l_{radio} = \tau_{sch} + \tau_{data} + \tau_{HARQ} + N(\tau'_{sch} + \tau_{data} + \tau_{HARQ}), \quad (18)$$

where τ_{sch} represents the resource scheduling latency, τ_{data} denotes the data transmission latency, and τ_{HARQ} can be regarded as a fixed latency C [49]. According to [48], the transmission process is modeled as an M/M/1 queue. The resource scheduling latency is viewed as the queuing time, while the data transmission latency is treated as the service time. It is assumed that data arrivals follow a Poisson distribution with parameter λ_1 , and the service time follows an exponential distribution with parameter λ_2 , denote $\tau_{tx} = \tau_{sch} + \tau_{data} + C$

⁵<https://genesys-offenburg.de/adma-g/>

represents the processing and transmission latency, while the arrival of data packets can be represented as a Poisson process

$$\begin{aligned} P(N = n | \tau_{\text{tx}} = t) &= \frac{P(N = n) P(\tau_{\text{tx}} | N = n)}{P(\tau_{\text{tx}} = t)} \\ &= \frac{1}{P(\tau_{\text{tx}} = t)} P_n \frac{\lambda_2 e^{-\lambda_2 t} (\lambda_2 t)^{n-1}}{n!} \\ &= \frac{(1 - \frac{\lambda_1}{\lambda_2}) \lambda_2 e^{-\lambda_2 t} (\lambda_1 t)^n}{P(\tau_{\text{tx}} = t) n!}. \end{aligned} \quad (19)$$

According to the theory of Poisson processes in stochastic process theory, the inter-arrival time between Poisson-distributed events follows an exponential distribution. Therefore, the probability of the transmission latency can be expressed as

$$P(\tau_{\text{tx}}) = (\lambda_2 - \lambda_1) e^{-(\lambda_2 - \lambda_1)t}. \quad (20)$$

According to Equation 20, the distribution of the transmission latency follows an exponential distribution with parameter $\mu_1 = \lambda_2 - \lambda_1$. For the retransmission process, assuming the retransmission success probability is p , the probability of the first $n - 1$ times transmissions failing and the n^{th} transmission succeeding can be expressed as $P(N = n) = (1-p)^{n-1}p$. The number of retransmissions follow geometric distribution $N \sim \text{GE}(p)$, where p depends on the block error rate (BLER). Hence, the retransmission time τ_{rtx} follows the exponential distribution with rate parameter μ_2 . Considering that the BLER is generally small, the focus is on cases where the number of retransmissions is 1. Thus, Equation 18 can be simplified to

$$l_{\text{radio}} = \tau_l \approx \tau_{\text{tx}} + \tau_{\text{rtx}_1} p_1. \quad (21)$$

Based on the above derivation, the random variable l_{radio} can be viewed as the sum of two independent random variables, τ_{tx} and τ_{rtx_1} that follow exponential distributions. Therefore, its probability density function can be expressed as

$$\begin{aligned} f_{\text{radio}}(\tau_l) &= \int_{-\infty}^{\infty} p_{\text{tx}}(\tau) p_{\text{rtx}_1}(\tau_l - \tau) d\tau \\ &= \int_0^{\tau_l} \mu_1 e^{-\mu_1 \tau} \mu_2 e^{-\mu_2 (\tau_l - \tau)} d\tau \\ &= \mu_1 \mu_2 e^{-\mu_2 \tau_l} \int_0^{\tau_l} e^{-(\mu_1 - \mu_2) \tau} d\tau. \end{aligned} \quad (22)$$

Without loss of generality, it is assumed that the retransmission latency is approximately equal to the latency of the first transmission. Relations $\tau_{\text{tx}} \sim \text{Exp}(\mu_1)$, $\tau_{\text{rtx}_1} \sim \text{Exp}(\mu_2)$, $\mu = \mu_1 = \mu_2$ can be established. Equation 22 can be rewritten as

$$f_{\text{radio}}(\tau_l) = \mu^2 e^{-\mu \tau_l} \int_0^{\tau_l} 1 d\tau = \mu^2 \tau_l e^{-\mu \tau_l}, \quad (23)$$

which is equivalent to the probability distribution of $l_{\text{radio}} \sim \text{Gamma}(2, \mu)$. Therefore, the communication latency statistical model for 5G E2E theoretically follows a **Gamma distribution**.

REFERENCES

- [1] SAE, *Taxonomy and Definitions for Terms Related to Cooperative Driving Automation for On-Road Motor Vehicles*, Std., 2021, issued by the Cooperative Driving Automation (CDA) Committee, Last accessed: October 24, 2024.
- [2] W. Chu, Q. Wuniri, X. Du, Q. Xiong, T. Huang, and K. Li, "Cloud control system architectures, technologies and applications on intelligent and connected vehicles: a review," *Chinese Journal of Mechanical Engineering*, vol. 34, no. 1, p. 139, 2021.
- [3] USDOT, "Saving lives with connectivity: A plan to accelerate v2x deployment," https://www.its.dot.gov/research_areas/emerging_tech/pdf/Accelerate_V2X_Deployment_final.pdf, 2024, U.S. Department of Transportation, Office of the Assistant Secretary for Research and Technology, Last accessed: October 24, 2024.
- [4] E. Thorn, S. Kimmel, and M. Chaka, "A framework for automated driving system testable cases and scenarios," National Highway Traffic Safety Administration, Washington, DC, Report DOT HS 812 623, September 2018, report No. DOT HS 812 623.
- [5] N. Kalra and S. M. Paddock, "Driving to safety: How many miles of driving would it take to demonstrate autonomous vehicle reliability?" *Transportation Research Part A: Policy and Practice*, vol. 94, pp. 182–193, 2016.
- [6] D. Arminas, "Zalazone test track gears up," 2020, accessed: 2024-07-29. [Online]. Available: <https://www.worldhighways.com/news/zalazone-test-track-gears>
- [7] V. G. Cerf, "A comprehensive self-driving car test," *Commun. ACM*, vol. 61, no. 2, p. 7, jan 2018.
- [8] Y. Li, W. Yuan, S. Zhang, W. Yan, Q. Shen, C. Wang, and M. Yang, "Choose your simulator wisely: A review on open-source simulators for autonomous driving," *IEEE Transactions on Intelligent Vehicles*, pp. 1–19, 2024.
- [9] A. Choudhury, T. Maszczyk, M. T. Asif, N. Mitrovic, C. B. Math, H. Li, and J. Dauwels, "An integrated v2x simulator with applications in vehicle platooning," in *2016 IEEE 19th International Conference on Intelligent Transportation Systems (ITSC)*, 2016, pp. 1017–1022.
- [10] A. Choudhury, T. Maszczyk, C. B. Math, H. Li, and J. Dauwels, "An integrated simulation environment for testing v2x protocols and applications," *Procedia Computer Science*, vol. 80, pp. 2042–2052, 2016.
- [11] H. Hu, R. Chai, M. Chen, and X. Yang, "System-level simulation platform of c-v2x mode 4: Integrating carmaker and ns-3," in *2021 IEEE 32nd Annual International Symposium on Personal, Indoor and Mobile Radio Communications (PIMRC)*, 2021, pp. 1457–1462.
- [12] D. Jia, J. Sun, A. Sharma, Z. Zheng, and B. Liu, "Integrated simulation platform for conventional, connected and automated driving: A design from cyber-physical systems perspective," *Transportation Research Part C: Emerging Technologies*, vol. 124, p. 102984, 2021.
- [13] T. Harges, I. Turcanu, and C. Sommer, "Poster: A case for heterogeneous co-simulation of cooperative and autonomous driving," in *2023 IEEE Vehicular Networking Conference (VNC)*, 2023, pp. 151–152.
- [14] A. Eichberger, G. Markovic, Z. Magosi, B. Rogic, C. Lex, and S. Samiec, "A car2x sensor model for virtual development of automated driving," *International Journal of Advanced Robotic Systems*, vol. 14, no. 5, p. 1729881417725625, 2017.
- [15] S. Feng, Y. Feng, X. Yan, S. Shen, S. Xu, and H. X. Liu, "Safety assessment of highly automated driving systems in test tracks: A new framework," *Accident Analysis & Prevention*, vol. 144, p. 105664, 2020.
- [16] G. Lee, S. Ha, and J.-i. Jung, "Integrating driving hardware-in-the-loop simulator with large-scale vanet simulator for evaluation of cooperative eco-driving system," *Electronics*, vol. 9, no. 10, 2020.
- [17] S. Peters, F. Sivrikaya, and X.-T. Dang, "Sep4cam - a simulative / emulative platform for c-v2x application development in cross-border and cross-domain environments," in *2021 IEEE/ACM 25th International Symposium on Distributed Simulation and Real Time Applications (DS-RT)*, 2021, pp. 1–4.
- [18] J. Lei, S. Chen, L. Zeng, F. Liu, K. Zhu, and J. Liu, "In-chamber v2x oriented test scheme for connected vehicles," in *2019 IEEE Intelligent Vehicles Symposium (IV)*, 2019, pp. 1–6.
- [19] J. Wang and Y. Zhu, "A hardware-in-the-loop v2x simulation framework: Cartest," *Sensors*, vol. 22, no. 13, 2022.
- [20] C. Olaverri-Monreal, J. Errea-Moreno, A. Díaz-Álvarez, C. Biurrun-Quel, L. Serrano-Arriezu, and M. Kuba, "Connection of the sumo microscopic traffic simulator and the unity 3d game engine to evaluate v2x communication-based systems," *Sensors*, vol. 18, no. 12, 2018.

- [21] T.-K. Lee, T.-W. Wang, W.-X. Wu, Y.-C. Kuo, S.-H. Huang, G.-S. Wang, C.-Y. Lin, J.-J. Chen, and Y.-C. Tseng, "Building a v2x simulation framework for future autonomous driving," in *2019 20th Asia-Pacific Network Operations and Management Symposium (APNOMS)*, 2019, pp. 1–6.
- [22] B. Senkus and M. Soyurk, "Multi-user real-time controllable connected cars testing platform," in *2023 IEEE International Automated Vehicle Validation Conference (IAVVC)*, 2023, pp. 1–6.
- [23] M. Jooriah, D. Datsenko, J. Almeida, A. Sousa, J. Silva, and J. Ferreira, "A co-simulation platform for v2x-based cooperative driving automation systems," in *2024 IEEE Vehicular Networking Conference (VNC)*, 2024, pp. 227–230.
- [24] R. Xu, Y. Guo, X. Han, X. Xia, H. Xiang, and J. Ma, "Opencda: An open cooperative driving automation framework integrated with co-simulation," in *2021 IEEE International Intelligent Transportation Systems Conference (ITSC)*, 2021, pp. 1155–1162.
- [25] D. Nalic, A. Eichberger, G. Hanzl, M. Fellendorf, and B. Rogic, "Development of a co-simulation framework for systematic generation of scenarios for testing and validation of automated driving systems," in *2019 IEEE Intelligent Transportation Systems Conference (ITSC)*, 2019, pp. 1895–1901.
- [26] E. Zhang and N. Masoud, "V2xsim: A v2x simulator for connected and automated vehicle environment simulation," in *2020 IEEE 23rd International Conference on Intelligent Transportation Systems (ITSC)*, 2020, pp. 1–6.
- [27] J. Hu, X. Yan, G. Wang, M. Tu, X. Zhang, H. Wang, D. Gruyer, and J. Lai, "A simulation platform for truck platooning evaluation in an interactive traffic environment," *IEEE Transactions on Intelligent Transportation Systems*, pp. 1–20, 2024.
- [28] B. Mafakheri, P. Gonnella, A. Bazzi, B. M. Masini, M. Caggiano, and R. Verdone, "Optimizations for hardware-in-the-loop-based v2x validation platforms," in *2021 IEEE 93rd Vehicular Technology Conference (VTC2021-Spring)*, 2021, pp. 1–7.
- [29] G. Gemmi, P. Johari, P. Casari, M. Polese, T. Melodia, and M. Segata, "Colossumo: Evaluating cooperative driving applications with colossum;" 2024.
- [30] L. Bonati, P. Johari, M. Polese, S. D'Oro, S. Mohanti, M. Tehrani-Moayyed, D. Villa, S. Shrivastava, C. Tassie, K. Yoder, A. Bagga, P. Patel, V. Petkov, M. Seltser, F. Restuccia, A. Gosain, K. R. Chowdhury, S. Basagni, and T. Melodia, "Colosseum: Large-scale wireless experimentation through hardware-in-the-loop network emulation," in *2021 IEEE International Symposium on Dynamic Spectrum Access Networks (DySPAN)*, 2021, pp. 105–113.
- [31] SAE J3016, *Taxonomy and Definitions for Terms Related to On-Road Motor Vehicles*, Std. SAE J3016, 2018, last accessed: October 24, 2024.
- [32] M. C. Lucas-Estañ, B. Coll-Perales, T. Shimizu, J. Gozalvez, T. Higuchi, S. Avedisov, O. Altintas, and M. Sepulcre, "An analytical latency model and evaluation of the capacity of 5g nr to support v2x services using v2n2v communications," *IEEE Transactions on Vehicular Technology*, vol. 72, no. 2, 2023.
- [33] B. Coll-Perales, M. C. Lucas-Estañ, T. Shimizu, J. Gozalvez, T. Higuchi, S. Avedisov, O. Altintas, and M. Sepulcre, "End-to-end v2x latency modeling and analysis in 5g networks," *IEEE Transactions on Vehicular Technology*, vol. 72, no. 4, pp. 5094–5109, 2023.
- [34] D. Ficzer, G. Soos, and P. Varga, "A compact 5g non-public network," in *2021 17th International Conference on Network and Service Management (CNSM)*. IEEE, 2021, pp. 518–520.
- [35] D. Ficzer, G. Soós, P. Varga, and Z. Szalay, "Real-life v2x measurement results for 5g nsa performance on a high-speed motorway," in *2021 IFIP/IEEE International Symposium on Integrated Network Management (IM)*, 2021, pp. 836–841.
- [36] J. Reckenzaun, R. Rott, M. Kirchengast, D. J. Ritter, P. Innerwinkler, S. Solmaz, C. Pilz, M. Schratler, A. Eichberger, T. Mihalj *et al.*, "Transnational testing, operation and certification of automated driving systems: Perspective from teststeps and central system eureka projects-mid-term results," in *2023 IEEE International Automated Vehicle Validation Conference (IAVVC)*. IEEE, 2023, pp. 1–8.
- [37] V. Tihanyi, A. Rövid, V. Remeli, Z. Vincze, M. Csonthó, Z. Pethő, M. Szalai, B. Varga, A. Khalil, and Z. Szalay, "Towards cooperative perception services for its: Digital twin in the automotive edge cloud," *Energies*, vol. 14, no. 18, p. 5930, 2021.
- [38] V. Tihanyi, T. Tettamanti, M. Csonthó, A. Eichberger, D. Ficzer, K. Gangel, L. B. Hörmann, M. A. Klaffenböck, C. Knauder, P. Luley *et al.*, "Motorway measurement campaign to support r&d activities in the field of automated driving technologies," *Sensors*, vol. 21, no. 6, p. 2169, 2021.
- [39] A. Rovid, V. Tihanyi, M. Cserni, M. Csontho, A. Domina, V. Remeli, Z. Vincze, M. Szanto, M. Szalai, S. Nagy *et al.*, "Digital twin and cloud based remote control of vehicles," in *2024 IEEE International Conference on Mobility, Operations, Services and Technologies (MOST)*. IEEE, 2024, pp. 154–167.
- [40] X. Zhang, L. Xiong, P. Zhang, B. Leng, and Y. Che, "Cloud control with communication delay prediction for intelligent connected vehicles," in *2024 IEEE Intelligent Vehicles Symposium (IV)*. IEEE, 2024, pp. 539–544.
- [41] P. Junietz, F. Bonakdar, and B. Klamann, "PEGASUS Bericht: Kritikalitätsmetriken," Institute of Automotive Engineering (FZD), Darmstadt, Technical Report, 2018.
- [42] A. Várhelyi, "Drivers' speed behaviour at a zebra crossing: a case study," *Accident Analysis & Prevention*, vol. 30, no. 6, pp. 731–743, 1998.
- [43] ISO 2631, *Mechanical Vibration and Shock – Evaluation of Human Exposure to Whole-Body Vibration*, Std. ISO 2631-1:1997, 2001, last accessed: October 24, 2024.
- [44] Y. Zhao, W. Xiao, T. Mihalj, J. Hu, and A. Eichberger, "Chat2scenario: Scenario extraction from dataset through utilization of large language model," in *2024 IEEE Intelligent Vehicles Symposium (IV)*, 2024, pp. 559–566.
- [45] D. Kollreider, "Identifikation der reifeneigenschaften als grundlage zur fahrdynamikbewertung," Ph.D. dissertation, Graz University of Technology, Graz, Austria, 2009.
- [46] F. M. Leichtfried, "Parameterbestimmung von vereinfachten fahrdynamikmodellen anhand ausgewählter fahrmanöver," Master's thesis, Graz University of Technology, Graz, Austria, 2015.
- [47] E. Reichmann-Blaga, "Validierung von fahrzeugdynamischen simulationsmodellen anhand von fahrzeugmessungen," Master's thesis, Graz University of Technology, Graz, Austria, 2024.
- [48] B. Coll-Perales, M. C. Lucas-Estañ, T. Shimizu, J. Gozalvez, T. Higuchi, S. Avedisov, O. Altintas, and M. Sepulcre, "End-to-end v2x latency modeling and analysis in 5g networks," *IEEE Transactions on Vehicular Technology*, vol. 72, no. 4, pp. 5094–5109, 2022.
- [49] M. Skocaj, F. Conserva, N. S. Grande, A. Orsi, D. Micheli, G. Ghinamo, S. Bizzari, and R. Verdone, "Data-driven predictive latency for 5g: A theoretical and experimental analysis using network measurements," in *2023 IEEE 34th Annual International Symposium on Personal, Indoor and Mobile Radio Communications (PIMRC)*. IEEE, 2023, pp. 1–6.